



---

# Liquefaction and Non-liquefaction Cases from the Mataquito Bridge, Chile, after the $M_w$ 8.8 (2010) and $M_w$ 6.6 (2019) Earthquakes

**Ricardo Moffat**, Civil Engineer, Universidad Adolfo Ibáñez, Santiago, Chile; email: [ricardo.moffat@uai.cl](mailto:ricardo.moffat@uai.cl)

**Robb Moss**, Civil Engineer, California Polytechnic State University, San Luis Obispo, USA; email: [rmoss@calpoly.edu](mailto:rmoss@calpoly.edu)

**ABSTRACT:** *This paper describes field investigations and soil foundation performance of the Mataquito Bridge with respect to the 2010  $M_w$  8.8 and 2019  $M_w$  6.6 Chilean earthquakes. The Mataquito Bridge was constructed at the site prior to both earthquakes using a pile foundation designed against liquefaction and lateral spreading. The foundation system performed correctly during both earthquakes, and in the case of the 2010 event it withstood surface manifestation of liquefaction and lateral spreading loads. Different liquefaction severity indices are used to assess the liquefaction hazard with data from in-situ measurements. This paper provides a collection of data ( $V_s$ , CPT, SPT) for liquefaction and non-liquefaction cases at the same site under two different levels of shaking, and valuable case history data for future triggering and severity index models. Lateral displacements are also calculated and compared with those observed on the field after the 2010 earthquake.*

**KEYWORDS:** liquefaction; lateral displacement; seismic settlement

**SITE LOCATION:** [Geo-Database](#)

## INTRODUCTION

Typical effects of strong earthquakes are ground shaking, ground rupture, land-slides, tsunamis, and liquefaction. In Mavroulis et al. (2021) and Liu et al. (2021) are shown examples of these effects on soil structures due to liquefaction and other causes. In a seismic country such as Chile, these effects have been observed for various large earthquakes and structures. One of these structures is the Mataquito Bridge. This bridge is a 320 m long bridge located close to Curepto along the coast of the El Maule Region of Chile ( $35.05^\circ$ ,  $72.16^\circ$  WGS84). This structure allows public transit over the Mataquito River along Highway 160. The Mataquito River is 95 km long and has a water flow volume that varies between 20,000 and 230,000 m<sup>3</sup>/s between summer and spring on a normal year. The original soil mechanic report (Petrus Consultores, 2006), predicted that there was susceptibility to liquefaction of the upper soil strata of an approximate 5 m thickness based on subsurface exploration performed during the years 1997, 2002, and 2005. The design therefore considered the use of three circular piles (1 m in diameter) below each pier to pass through the liquefiable layer, a dense sand layer, and penetrate at least 1 m on a competent gravel located at approximately 14 m deep. Scour design is also an important aspect to be considered, as it is well-understood that foundations subjected to hydraulic actions can lead to scour hole formation and reduction of embedment.

This bridge behaved adequately during the large 2010  $M_w$  8.8 Maule earthquake; its structure remained undamaged and functional with insignificant residual displacements. Additional details of the behavior of the Mataquito Bridge after the  $M_w$  8.8 Maule earthquake can be found in Bray et al. (2010) and Ledezma et al. (2012). Also, a dynamic modeling of the Mataquito Bridge affected by liquefaction is presented in Gutierrez and Ledezma (2007). Lateral spreading was observed beneath the bridge parallel to the river, with displacements in the order of 50 cm to 200 cm. The approach embankment on the north side of the bridge settled up to 70 cm Elnashai et al. (2011). In this current paper, the behavior of the bridge foundation soil is analyzed for two earthquakes: the  $M_w$  8.8 2010 and the  $M_w$  6.6 2019 earthquakes. Regarding the former, clear evidence of liquefaction was observed; in the latter, no evidence of liquefaction was observed. A new soil exploration was performed on site acquiring CPT soundings, downhole tests, and MASW profiles along the north and south approaches

Submitted: 20 March 2022; Published: 21 December 2022

Reference: Moffat, R., and Moss, R. (2022). Liquefaction and Non-liquefaction Cases from the Mataquito Bridge, Chile, after the  $M_w$  8.8 (2010) and  $M_w$  6.6 (2019) Earthquakes. International Journal of Geotechnical Engineering Case Histories, Volume 7, Issue 3, pp. 1-17,



of the bridge. New and existing information was analyzed to explain the observed behavior of the soil. Figure 1 shows an overview map with the bridge location, earthquake epicenters, and location of seismic stations.

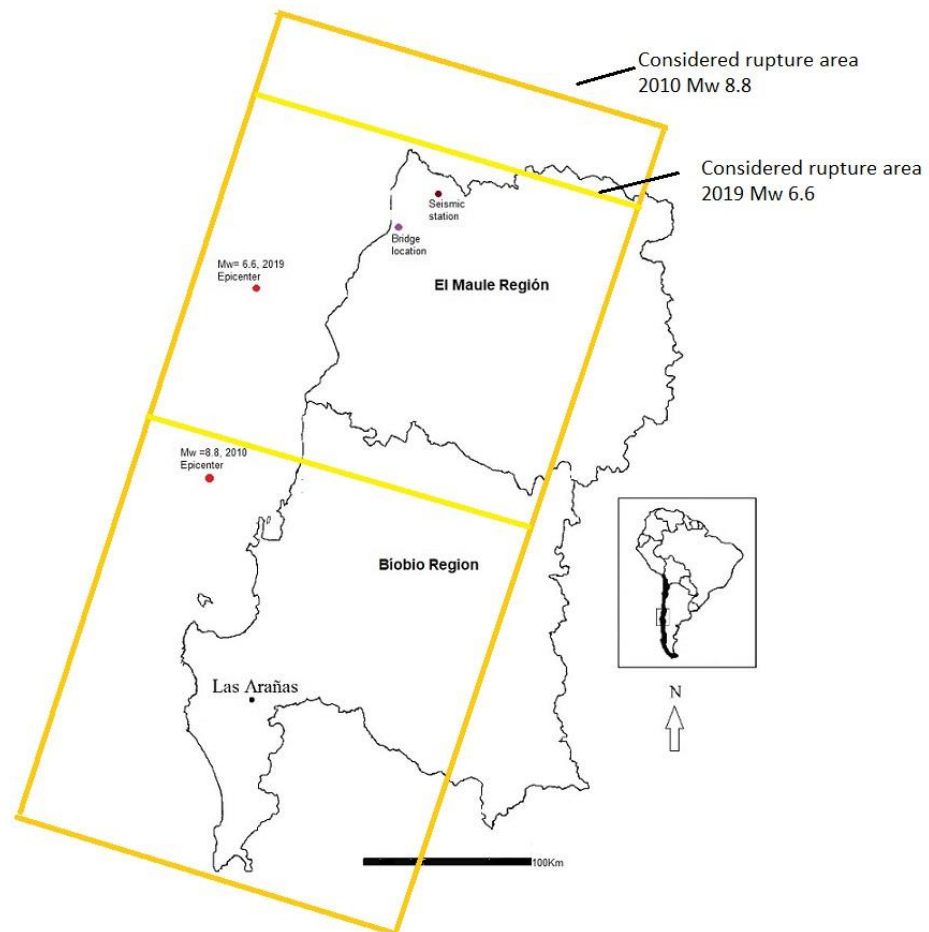


Figure 1. Overview map showing the epicenters of the 2010 and 2019 earthquakes, the location of the bridge, and the location of the nearby strong motion station.

## 2010 EARTHQUAKE AND OBSERVATIONS

The 2010  $M_w$  8.8 Maule, Chile earthquake is the 6th largest recorded earthquake ([www.usgs.gov](http://www.usgs.gov)). This great earthquake was heavily instrumented, and was recorded by strong motion and GPS instruments at different locations along the length of Chile. As with many earthquakes in Chile, the thrust movement was generated due to interaction between the South American plate and the subducting Nazca plate. The hypocenter has been located at  $(-36.29, -73.24^\circ \text{ WGS84})$  by the Chilean national seismological center ([www.sismologia.cl](http://www.sismologia.cl)). The earthquake's rupture length was roughly 450 km from south to north (Bray et al., 2010).

Damage to structures due to geotechnical ground failures were reported mainly for buildings, highways, bridges, and tailings dams (Bray et al., 2010, Elnashai et al., 2011, Yen et al., 2011). More than 120 sites were observed to have liquefied after the 2010 earthquake. These events were located from La Calera in the north to Valdivia in the south (about 1,000 km away from each other), with more spatially dense liquefaction manifestations reported in the southern extent in the Bío and Maule regions.

The closest strong motion record to the Mataquito Bridge site was located about 30 km further away from the epicenter in the upstream direction along the Mataquito River (northeast), and 215 km from the earthquake's epicenter at the town of Haulaño (Boroscsek et al., 2010). Maximum horizontal acceleration was 0.44 g on the west-east direction (see light line in

Figure 2) on a similar soil condition based on the distance to the Mataquito River. The Mataquito Bridge is located at approximately 190 km from the epicenter.

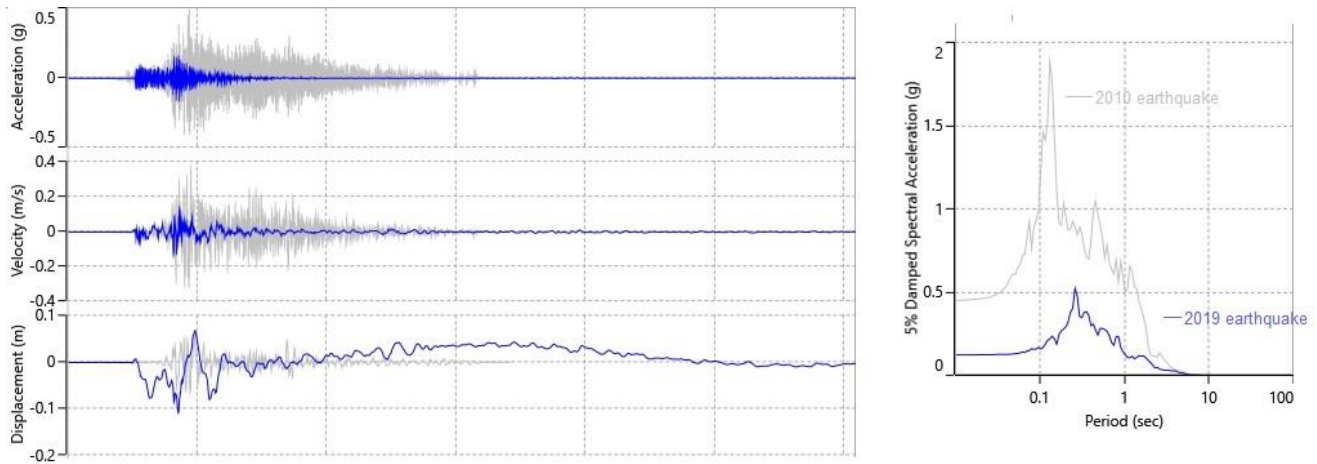


Figure 2. Strong ground motions and response spectra recorded at the 2010 Maule earthquake (lat. 36:17:23, lon. 73:14:20, Universidad de Chile, Ing. Civil), and 2019 earthquake (lat. -35.010, lon. -71.930, after Centro Sismológico Nacional, Universidad de Chile).

Reconnaissance of the bridge found large lateral spreads towards the river at the north and south abutments in adjacent fields and directly below the bridge deck. Figures 3, 4, and 5 show photos of the settlement and lateral spreading (with sand boils) on the north and south sides of the bridge. Lateral spreading on the south side appeared to be confined to the border of the river, with deformations decreasing rapidly around 20 m from the river's edge to the south. On the north side, due to the relatively flat topography, it was observed to extend up to 250 m from the river's edge. Evidence of settlement was observed on the approach embankment and the rows of piers. Cracking of the asphalt on the north side was also observed along a distance of 200 m from the river's edge along the road.



Figure 3. Lateral spreading at the north side of the bridge. Cracking showing roughly 0.6 m of vertical and 0.8 m of lateral displacement toward the river (Bray et al., 2010).



*Figure 4. Liquefaction effects along the south side of the bridge (Bray et al., 2010).*



*Figure 5. Sand boils observed in the cracks of lateral spreads, with the ejecta being fine sand (Bray et al., 2010).*



---

## 2019 EARTHQUAKE AND OBSERVATIONS

This later earthquake was observed on September 29<sup>th</sup>, 2019, and was  $M_w$  6.6. The closest accelerometer record for this earthquake is 25 km away from the bridge, and 130 km away from the epicenter of the earthquake, located between the towns of Haulaño and Licantén, and further away from the epicenter than the bridge (the bridge is at approximately 100 km from the epicenter). Maximum acceleration was 0.14g also in the west-east direction (see darker line in Figure 2).

This earthquake did not generate any major reported damage of consideration, as would be common in a seismic country like Chile. The site was visited before and after this earthquake by the authors. There was no evidence of liquefaction or changes on the surface. Figure 6 shows a photo of the north site during repeat CPT soundings after the 2019 earthquake.



*Figure 6. Photo of the north side after the 2019 earthquake (October 17<sup>th</sup>, 2019). The CPT truck is shown here doing subsurface testing.*

## PRIOR IN-SITU SOIL TESTING FROM 1996 TO 2005

An original subsurface investigation and geotechnical study was performed by a local geotechnical company (Petrus Consultores, 2006) in 1996 for a preliminary study, and again in 2005 for the definitive study. This soil exploration consisted of performing test pits along with rotary wash boring with a Standard Penetration Test (SPT) at different depths, with the typical sampling interval of 0.5 m to 2 m, depending on depth.

Results from these studies in terms of the interpreted stratigraphy, measured fine content, and SPT blow count are summarized directly from the original report in Figure 7 for the north side and Figure 8 for the south side of the bridge.

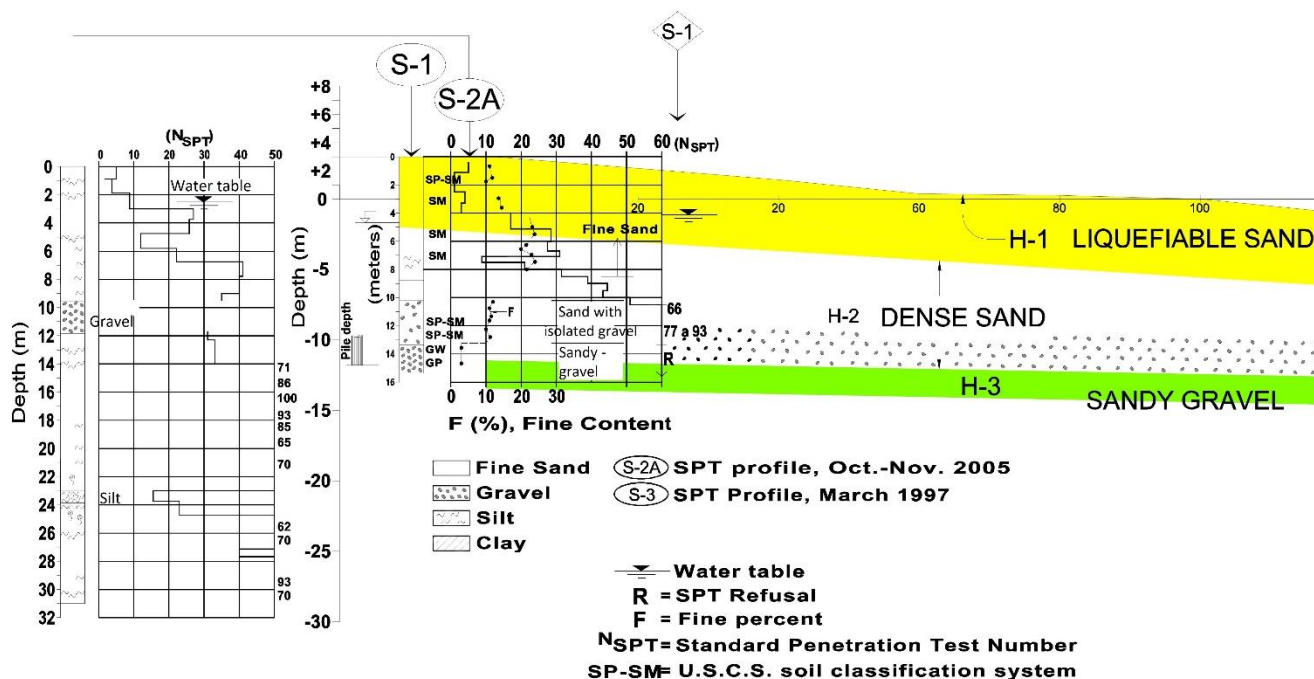


Figure 7. Subsurface information from the 1996 and 2005 investigations. The north side of the bridge is shown (modified from Petrus Consultores, 2006).

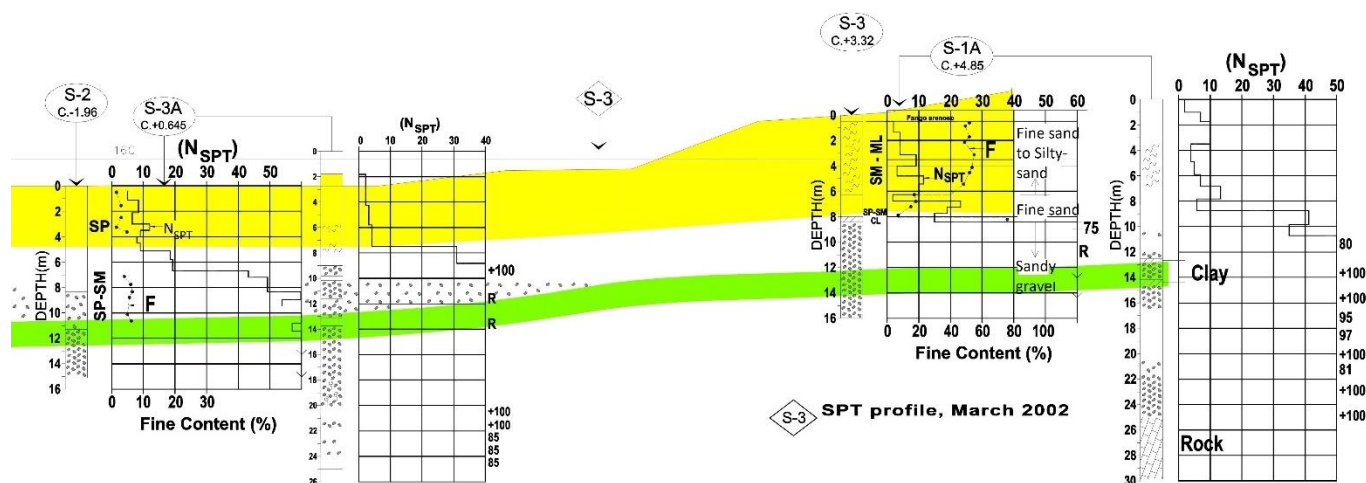


Figure 8. Subsurface information from the 1996 and 2005 investigations. The south side of the bridge is shown (modified from Petrus Consultores, 2006).

SPT testing was performed using an automatic hammer, but no energy measurements were performed. A hammer energy ratio (ER) = 0.8 is assumed to correct measured blow counts to  $N_{60}$ . From this data, it was originally deduced that the sand

layer up to a depth of 4 m to 6 m was susceptible to liquefaction (shown in Figures 7 and 8). According to this soil exploration, the upper sand layer has a variable non-plastic fines content between 1% and 25%. As a result of this, it was recommended to use piles that reach the dense gravelly sand at about 15 m below the surface, and thus mitigate liquefaction-induced foundation failure and/or large post-liquefaction settlements of the foundations.

During the 2010 earthquake, liquefaction and lateral spreading were observed in the north and south sides of the bridge. However, the design pile foundation was able to endure the observed liquefaction with only minor damage on the bridge.

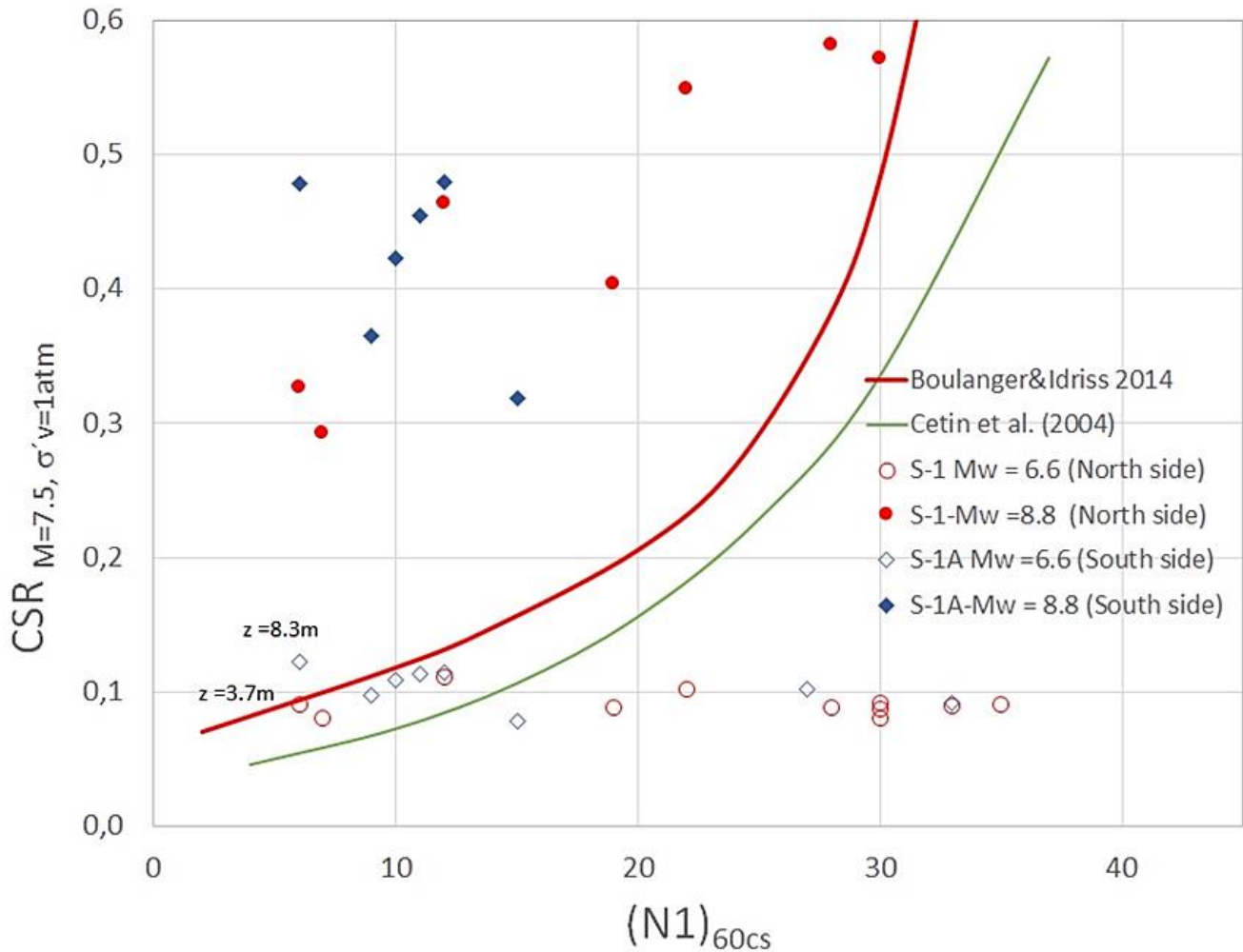


Figure 9. Liquefaction analysis with information prior to the 2010 earthquake.

Figure 9 shows the result of the liquefaction analysis using procedures (Cetin et al., 2004 and Boulanger and Idriss, 2014) with the original SPT data. Soil exploration S-1A was performed in the south side of the bridge, and soil exploration S-1 was performed in the north side. The NSPT blow count in both places are evaluated for the  $M_w$  8.8 2010 and  $M_w$  6.6 2019 earthquakes. Both soil explorations were located in places where the liquefaction manifestation was observed at the surface for the 2010 earthquake and no manifestation was observed for the 2019 earthquake. The evaluation for the 2010 earthquake using a PGA value of 0.44 g indicates potential liquefaction in both places (S-1 and S-1A) from depths just below the water table and down to a depth of 9 m. (Boroschek et al., 2012) proposed an attenuation relation for horizontal accelerations using the database of Chilean accelerograms located on different types of soils and recorded during earthquakes that occurred between 1985 and 2010. In Figure 10, this curve is shown together with another proposed by Zhao et al. (2006) using data from crustal and slab strong earthquakes recorded on soils. In both cases, at the rupture distance estimated for 2010 at the Mataquito Bridge, the PGA value is close to the 0.44 g used in this analysis. For the 2019 earthquake, a value of PGA equal to 0.14g was used for liquefaction evaluation. In this case, there is a border line point for data obtained at 3.7m deep at the



north side, and liquefaction potential is deduced at a depth of 8.3m in the south side (see Figure 9). This last case is probably too deep to exhibit liquefaction manifestation even if liquefaction was triggered at that depth (Ishihara, 1985 and Youd et al., 1995). Evaluation using both original data seems to correlate with field observations for both earthquakes, especially when considering the Boulanger and Idriss (2014) method.

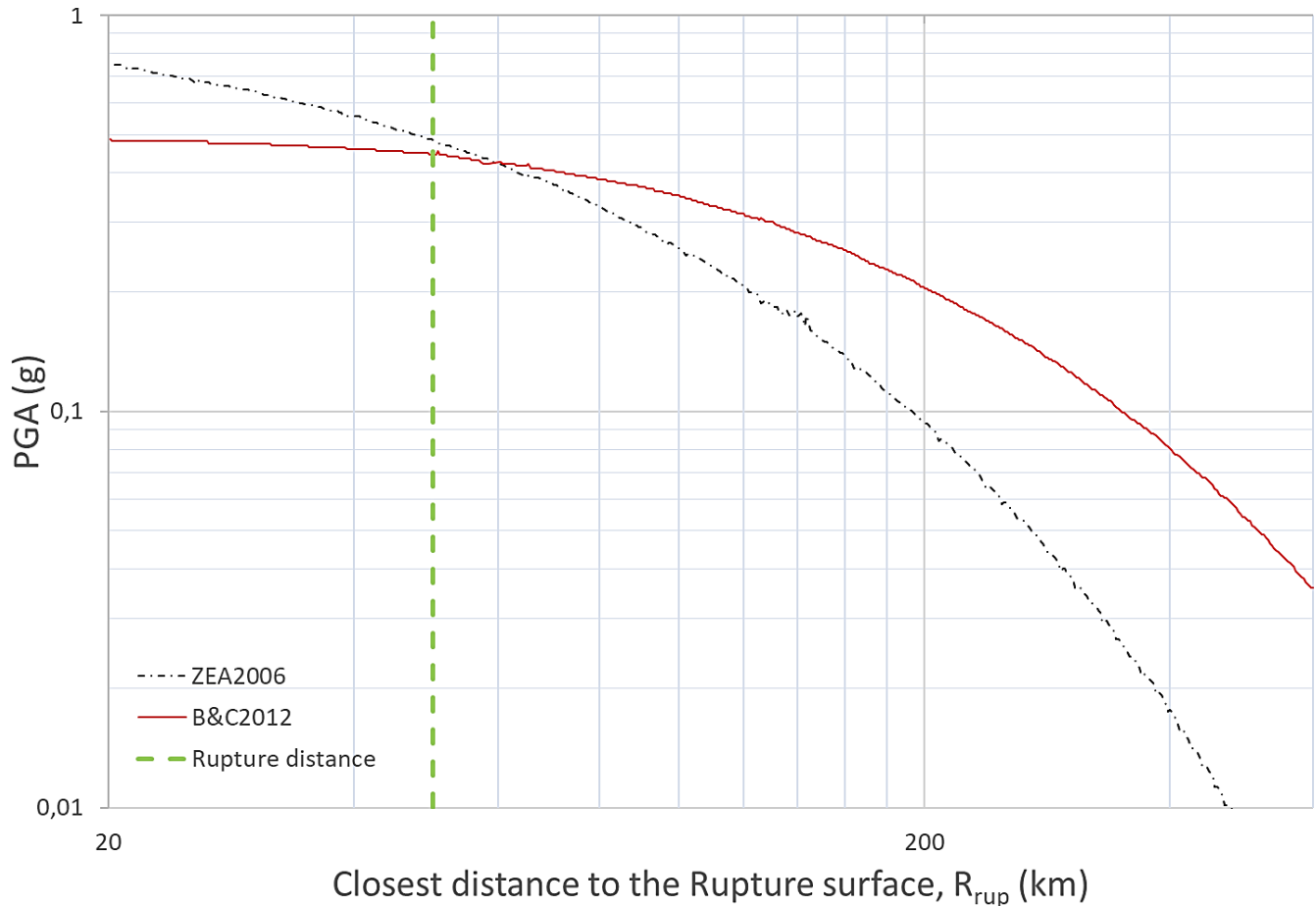


Figure 10. Attenuation relation for horizontal accelerations modified from Boroschek et al. (2012).

#### POSTERIOR IN-SITU TESTING DURING 2019

A new subsurface investigation campaign was performed at the end of 2019. This campaign consisted of seismic CPT soundings, multichannel analysis of surface waves (MASW), and soil sampling using the CPT rigs. CPT soundings were performed using a 22-ton truck ([www.lmmg.cl](http://www.lmmg.cl)) with a seismic piezocone penetrometer arrangement (Figure 6). The cones with a base area of 15 cm<sup>2</sup> and friction sleeve area of 225 cm<sup>2</sup> were used in this campaign, and were calibrated by Gregg Drilling in accordance to ASTM D5778-12 (2012). Pore pressure transducers were located behind the cone tip on the standard ( $u_2$ ) location. A geophone located inside the cone was used to collect seismic shear wave data. A total of 8 CPT soundings were performed to depths that varied between 7 m and just over 17 m where a dense gravel layer was encountered. The locations of CPT and MASW testing are shown in Figure 11.

MASW testing was performed using 24 vertical 4.5 Hz geophones and the ES-300 seismograph from geometrics. The distance between geophones was 1.25 m, and passive and active measurements were performed for the same linear arrangement in order to obtain a response across a broad range of frequencies. A shear wave velocity profile was deduced using MASW geophysics for the north side, starting at a location of CPT 7 in the direction of the center of the bridge. Another MASW line starting at CPT 2 to the direction of CPT 4 also generated a profile of  $V_s$  for the South side.



Figure 11. Posterior subsurface investigation locations from the 2019 field campaign.

## RESULTS AND LIQUEFACTION TRIGGERING EVALUATION

Liquefaction triggering was studied for both MASW profiles and downhole SCPT measurements using the procedure explained at Kayen et al. (2013). A 15% probability contour for initial liquefaction was considered as the deterministic boundary curve shown in Fig. 12. The results of this analysis, using MASW data, are shown in Fig. 12, where liquefaction is deduced from 3 m to 6 m at both sides of the river. Downhole CPT 3 is located at the south side of the bridge, and downhole CPT 8 is located at the north side. The analysis was performed for both earthquakes, where CPT 3 data was for depths between 1.5 m to 8.3 m, and CPT 8 was from 1.5 m to 6.3 m. The MASW and downhole shear wave velocity analysis seemed to correlate adequately with the observations from both earthquakes.

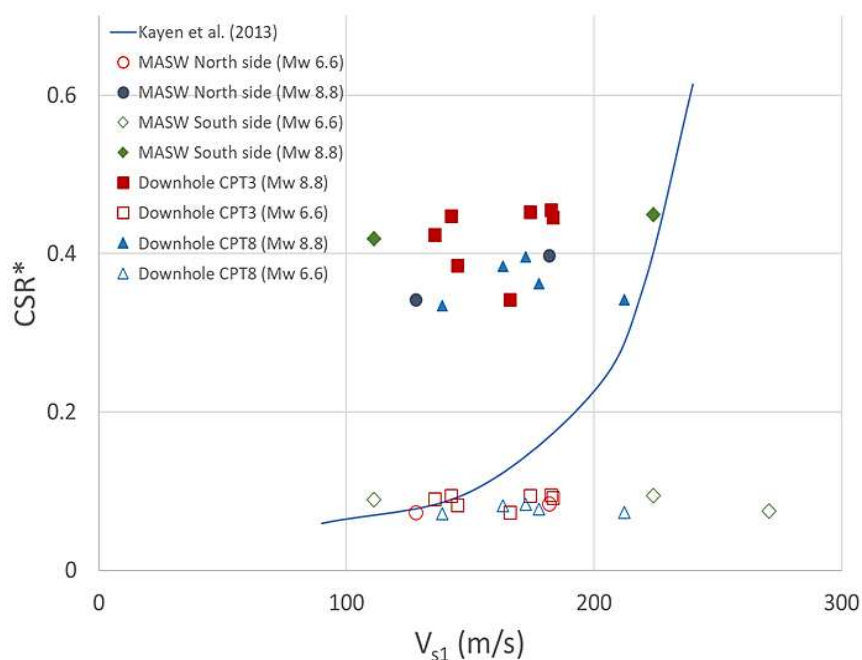


Figure 12. Liquefaction assessment using  $V_s$  from MASW and SCPT.

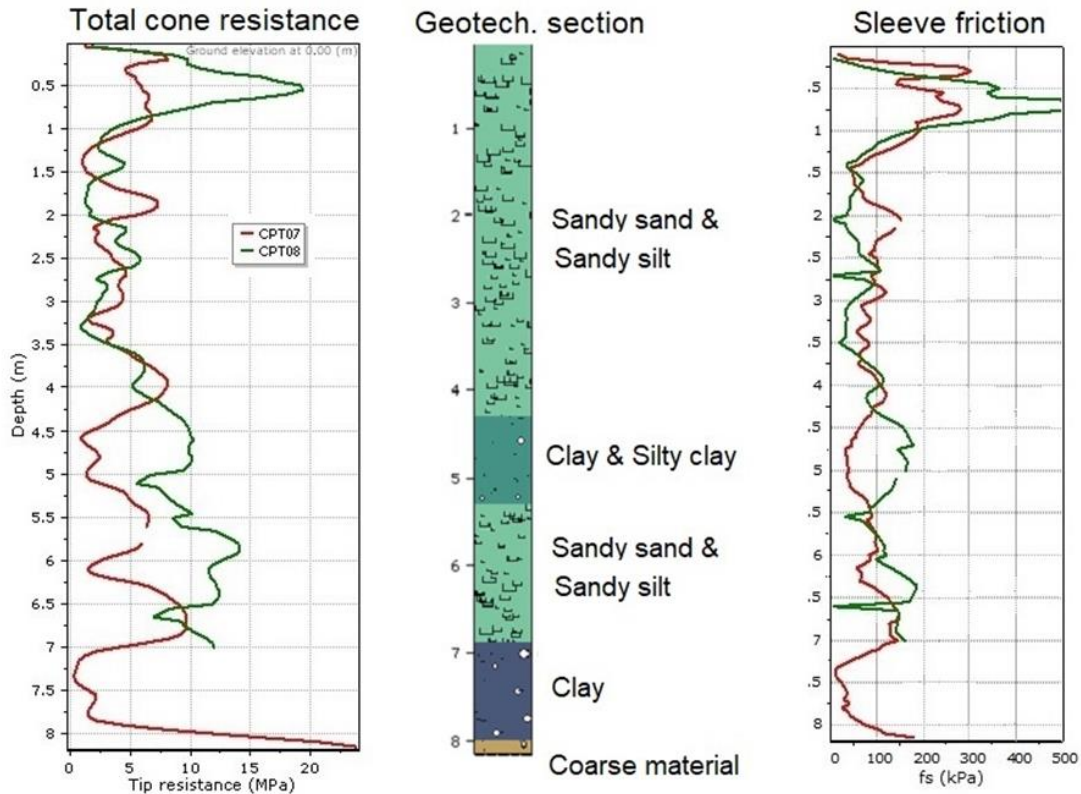


Figure 13. CPT soundings on the north side with the water table located at roughly at 2.5 m.

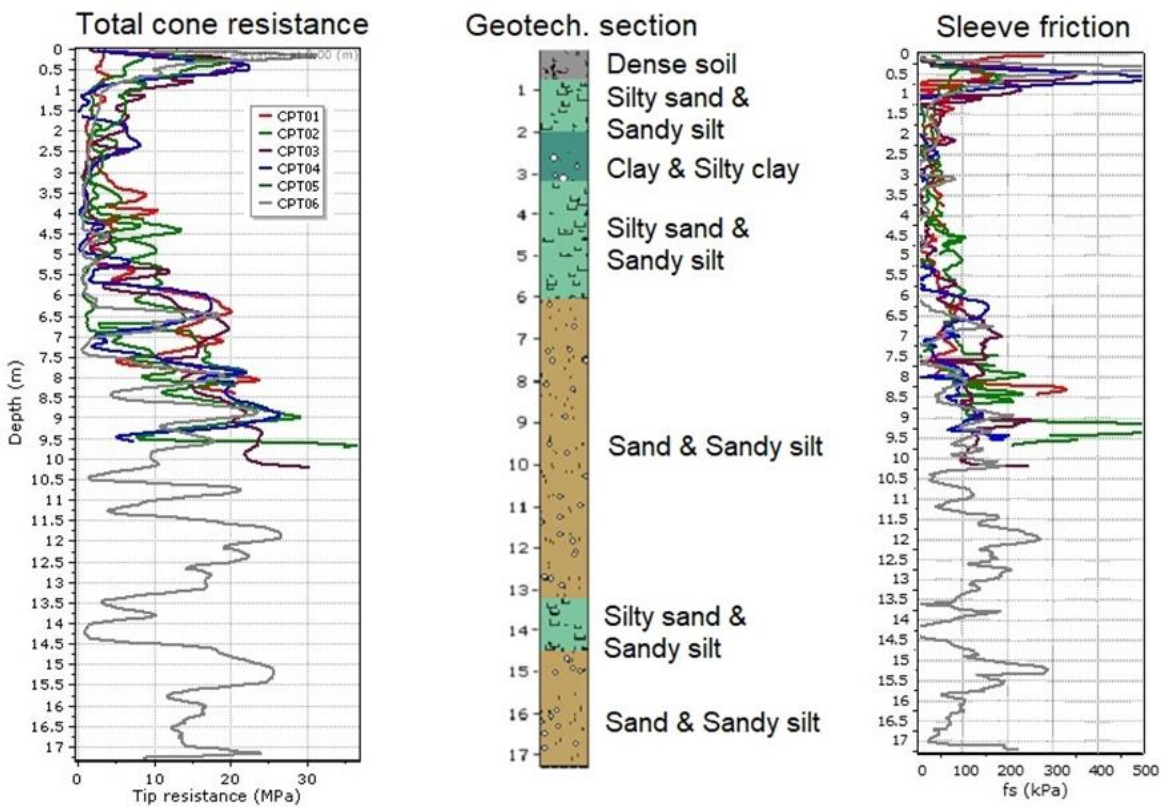


Figure 14. CPT soundings on the south side; the water table varies between 2 m to 5 m across the measured locations.



The liquefaction analysis using the CPT data and procedures Robertson and Wride (1997), Moss et al. (2006), and Boulanger and Idriss (2014) are shown in Figure 15. Boundary curves are deterministic or a 15% probability contour is used as deterministic. The analysis shown in this figure was performed for both earthquakes ( $M_w$  8.8 and  $M_w$  6.6), and used all CPT data until the gravel layer was reached. On the north side, the results agreed with what was observed in the field (see Figure 15). Liquefaction potential was deduced from the  $M_w$  8.8 earthquake for almost any depth. Regarding the  $M_w$  6.6, only a few points were on the liquefaction side, and these corresponded to depths between 7.3 m and 7.5 m, too deep to have a manifestation in surface of liquefaction (Ishihara, 1985, Youd et al., 1995).

Figure 16 shows the average values for an upper layer (between 2.5 m and 3.5 m) and lower layer (between 3.5 m and 6.5 m). In addition to the mean values shown in Figure 16, the standard deviation for calculated values of CSR and  $q_{c1Ncs}$  are also shown. The standard deviation of CSR was calculated following the methodology recommended by Cetin et al. (2018). As aforementioned, horizontal accelerations deduced from the attenuation relations and data from strong motion records relatively close to the Mataquito Bridge are consistent, and the coefficient of variation of maximum acceleration is assumed equal to 0.1. Ground water table standard deviation was assumed equal to 1 m. Moist and saturated unit weight were assumed to have a standard deviation equal to 0.5 kN/m<sup>3</sup>. Standard deviation of the participation factor ( $r_d$ ) was calculated according to Cetin and Seed (2004). On the other hand, standard deviation of  $q_{c1Ncs}$  was calculated from the actual data from CPT sounding measurements in each critical layer considered for the analysis. The results are consistent with what was observed on the field: liquefaction occurred during the 2010 earthquake, and no effects happened during the 2019 earthquake. The Zhang et al. (2002) method was used to estimate, from CPT data, the vertical settlements due to liquefaction. In order to obtain vertical settlement similar to what was observed on the field (20 to 30 cm), it is necessary to consider that both layers liquefied. Similarly, it will be shown later that lateral spreading would also need both layers to liquefy in order for the models to match the observed horizontal displacement.

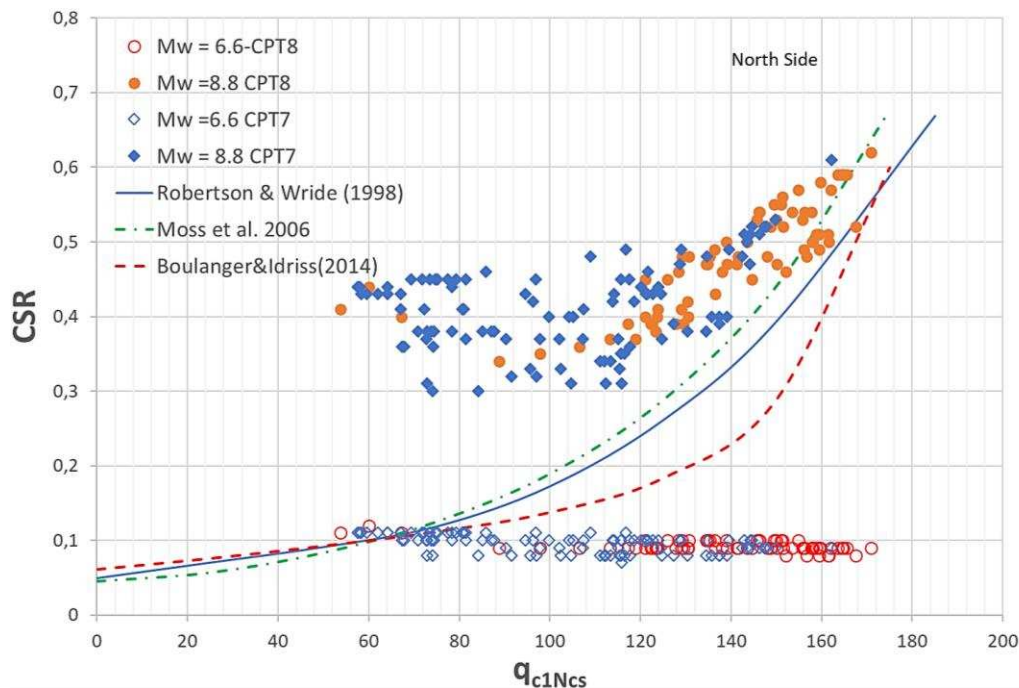


Figure 15. Liquefaction analysis on the north side (CPTs 7 and 8) with three triggering relationships.

On the south side, the results are similar to those of the north side. However, due to the topography, CPTs 4, 5, and 6 did not show liquefaction effects. The analysis of CPTs 1 to 3 considering the layer of similar CPT measurements is shown in Figure 17. The upper layer was chosen between 2.5 m and 4.95 m, and the lower layer between 5 m and 7.95 m.

It is possible to observe that many points (or depths) should have manifested liquefaction according to Boulanger and Idriss (2014); however, this was not observed on the field. The water table was found at 3.4 m and 5.2 m on CPTs 4 and 5 respectively. This could generate a considerable non-liquefiable layer that avoids manifestation of the phenomenon on the surface, as considered originally by Ishihara (1985).

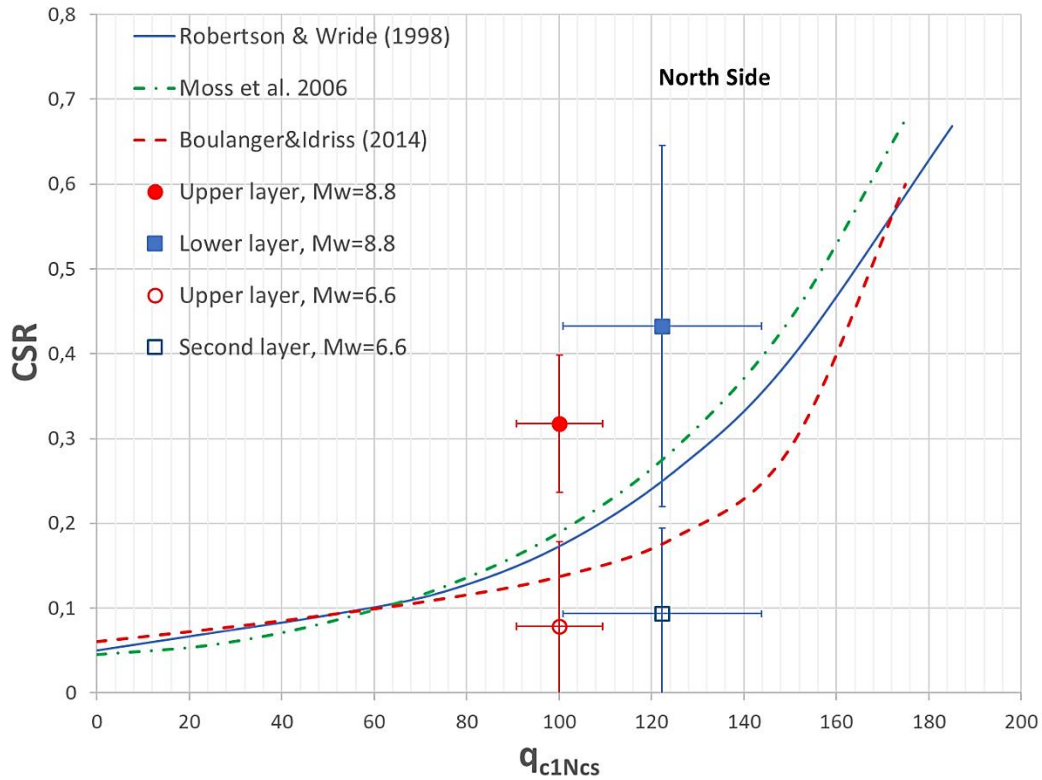


Figure 16. Liquefaction analysis on the north side; average values for CPTs 7 and 8 along with plus/minus one standard deviation.

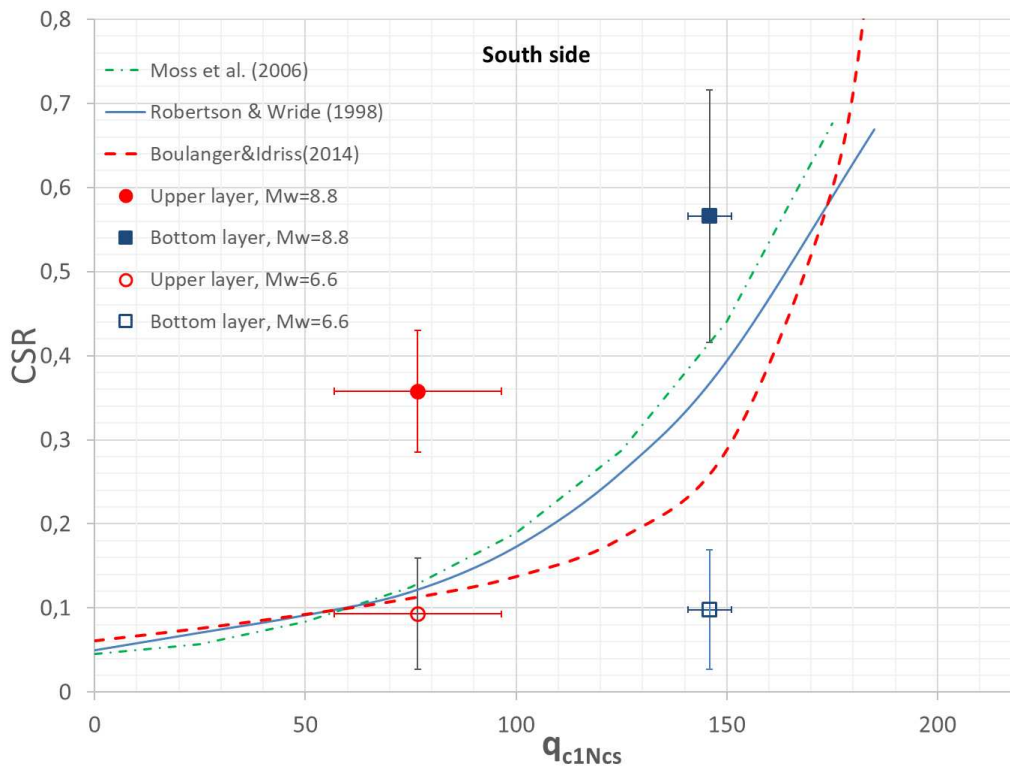


Figure 17. Liquefaction analysis on the south side; average values for CPTs 1 to 3 along with plus/minus one standard deviation.



The liquefaction analysis performed with data from CPTs 1 to 3 on the south side matches what was observed in the field. Special attention is given to the upper layer, as it is very close to the liquefaction triggering curve for the 2019 earthquake. Both Figures 16 and 17 show the standard deviation of CSR and  $q_{c1Ncs}$ , as previously explained.

Summary data from these two analyzed layers are shown in Tables 1 and 2, for the north and south sides of the bridge respectively.

*Table 1. Summary of liquefaction/non-liquefaction data on the north side.*

Event	Mw	Median critical Depth (m)	w.t. (m)	amax (g)	CSR*	±	qc1N,cs	±	Rf (%)	±	Liq.
2010 Earthquake	8,8	3	2	0,44	0,318	0,081	100,12	9,23	2,16	0,69	YES
2010 Earthquake	8,8	5	2	0,44	0,433	0,213	122,31	21,5	1,3	0,39	YES
2019 Earthquake	6,6	3	2	0,14	0,079	0,100	100,12	9,23	2,16	0,69	NO
2019 Earthquake	6,6	5	2	0,14	0,094	0,101	122,31	21,5	1,3	0,39	NO

*Table 2. Summary of liquefaction/non-liquefaction data on the south side.*

Event	Mw	Median critical Depth (m)	w.t. (m)	amax (g)	CSR*	±	qc1N,cs	±	Rf (%)	±	Liq.
2010 Earthquake	8,8	3,8	2,5	0,44	0,358	0,072	76,66	19,78	1,314	0,867	Yes
2010 Earthquake	8,8	6,5	2,5	0,44	0,566	0,15	145,92	5,12	0,724	0,367	Yes
2019 Earthquake	6,6	3,8	2,5	0,14	0,093	0,066	76,66	19,78	1,314	0,867	No
2019 Earthquake	6,6	6,5	2,5	0,14	0,098	0,071	145,92	5,12	0,724	0,367	No

### Surface Manifestation Index Evaluation

CPT data was also used to evaluate the surface manifestation, using an index such as: LPI,  $LPI_{ISH}$ , and LSN for all CPT soundings (Iwasaki et al., 1978, Maurer et al., 2015, Van Ballegooy et al., 2014). Figure 18 shows values of LSN, LPI, and  $LPI_{ISH}$ . Values of LPI and  $LPI_{ISH}$  are very sensitive when passing from the 2010 to the 2019 earthquake. According to this case history, LPI of 10 showed the liquefaction manifestation on the surface, and LPI of 0.5 did not. Calculated values of LPI and  $LPI_{ISH}$  for the 2019 earthquake were so low that they couldn't be observed in this figure. Similarly, values of  $LPI_{ISH}$  showed that for  $LPI_{ISH}$  of 6, there is liquefaction manifestation; for values lower than 0.2, however, liquefaction is not shown. On the other hand, LSN-calculated values showed that LSN above 15 liquefaction was observed—yet for values of LSN below 6.4, no liquefaction manifestation was observed.

Data from CPT 6—the CPT furthest south from the river's edge—is analyzed to show the possible variation of  $LPI_{ISH}$  with the main variables used for its liquefaction calculation, in order to check the robustness of the calculated values. A sensitivity analysis was performed for this sounding using fictional values of non-liquefaction layer (H1), fine content in depth, and PGA values to check for a possible effect of variation from the values derived from the in-situ soil exploration. The calculated average value of  $LPI_{ISH}$  was 11.2 with a standard deviation of 2.0. Similarly, for LSN, an average value of 26.4 and a standard deviation of 7.2 were obtained. For LPI, an average value of 20.0 and a standard deviation of 3.1 were obtained. Therefore, even a significant change in input values does not explain why there was no clear manifestation of liquefaction for the Mw 8.8 earthquake further away from the river's edge. One possible explanation is that the gravel layer, below the liquefied layer, and/or the ground slope are steeper further to the south from the river. And/or, this could be due to limitations of the simplified procedure used in this work to evaluate liquefaction. It has been shown that the use of the simplified method can overestimate or underestimate the potential of liquefaction as compared to a dynamic analysis of the soil. Correspondingly, assumptions such as horizontally layered soil profile, horizontal ground surface, and vertically propagating waves are not particularly accomplished at the location of CPT 6.

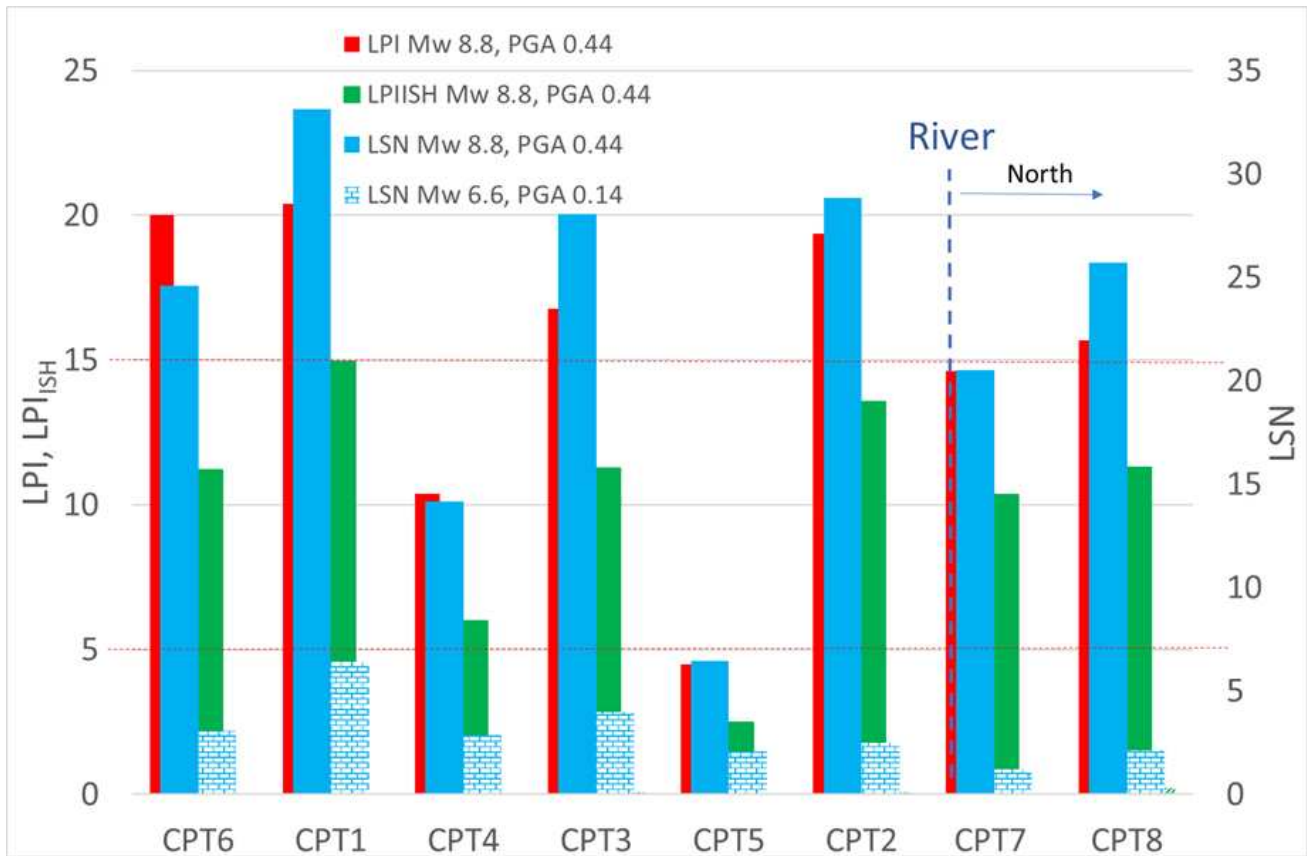


Figure 18. Liquefaction manifestation indexes; LSN, LPI, and LPI<sub>ISH</sub>.

### Lateral Spreading

Lateral spreading was observed for the 2010 earthquake, as was mentioned previously in this paper. Some of the most common deterministic methods to predict lateral displacement for gently sloping ground without a free face were used to deduce this movement. There is very little data from earthquakes with values of  $M_w$  above 8.0 to compare to these methods, therefore this case is used to compare observed displacement with deduced values (as shown in Figure 19).

The following data was used to calculate lateral displacement:

$R = 40$  km : horizontal distance to the rupture plane

$S = 3\%$  average ground slope

$T_{15} = 4.5$  m accumulated thickness where  $(N_1)_{60} < 15$

$F_{15} = 15\%$ : average fine content

$D_{50} = 0.4$  mm average grain size

$M_w = 8.8$

It is possible to observe that all methods (Zhang et al., 2002, Barlett and Youd, 1995, Youd et al., 1987, Hamada et al., 1987, Youd et al., 2002), with the exception of Barlett and Youd (1995) that was superseded by Youd et al. (2002), adequately predict the observed lateral displacement. This is consistent with what was mentioned by Youd et al. (2002), that erroneous data estimates were used on Barlett and Youd (1995). That caused this model to over-predict lateral spreading. Upper and lower layers were necessarily considered by these models to predict the observed displacement on the field. This confirms what was also aforementioned in this work: both layers must have liquefied during the 2020 earthquake.

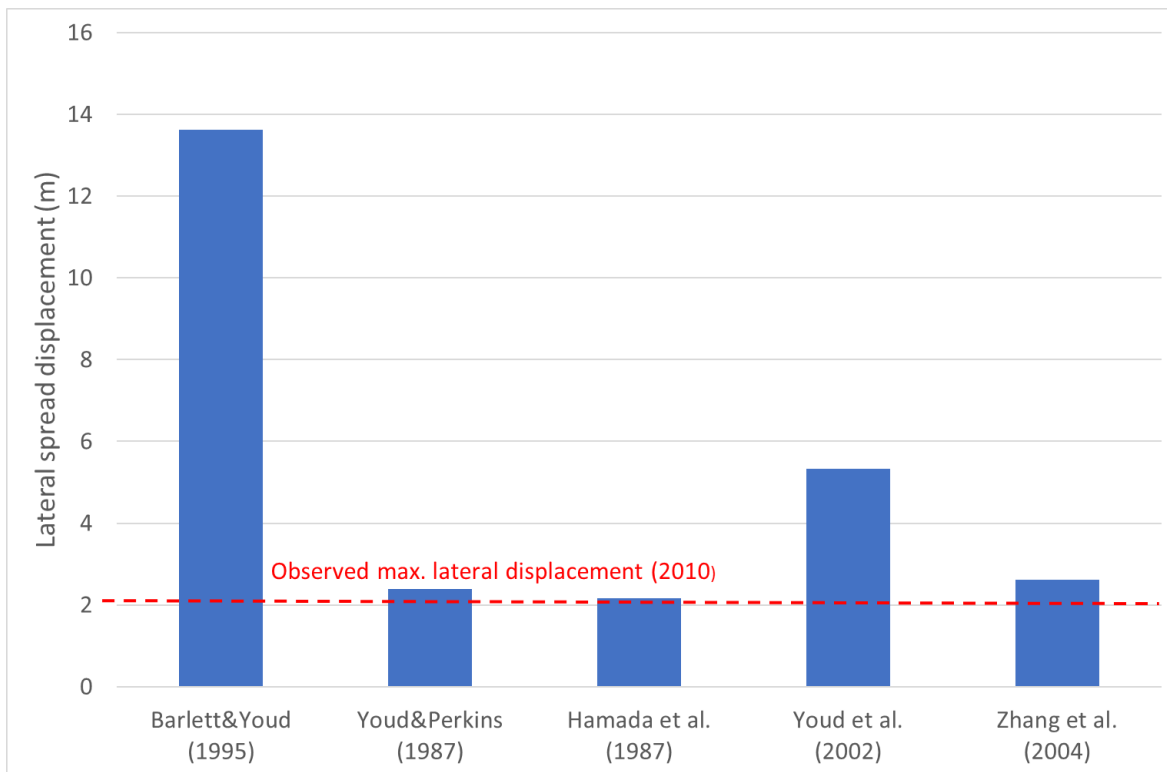


Figure 19. Calculated values of lateral displacement for different predictive models.

## CONCLUSION

This paper presents a case study from two large earthquakes with epicenters approximately the same distance from the Mataquito Bridge in Chile, where liquefaction was observed for the 2010  $M_w$  8.8 earthquake and no liquefaction was observed for the 2019  $M_w$  6.6 earthquake. The site was originally tested using rotary wash drilling with a Standard Penetration Test (SPT). The original geotechnical report considered liquefaction a hazard for the 1 m diameter piles that carry the bridge loads to depth. Liquefaction analysis was performed considering the original SPT data as well as new data obtained from seismic CPT soundings and MASW tests. Different triggering showed that the datasets in these cases were in the liquefaction side ( $M_w$  8.8) and non-liquefaction side ( $M_w$  6.6) of the triggering curves such as Robertson and Wride (1997), Cetin and Seed (2004), Moss et al. (2006), Boulanger and Idriss (2014, and Kayen et al. (2013). Data obtained prior to the 2010 earthquake (prior to liquefaction) and after both earthquakes (2010 and 2019) provided similar results in terms of the soil's susceptibility to liquefaction, and agree with field observations obtained after both earthquakes. The surface manifestation index analysis adequately showed what was clearly observed in the field for these two earthquakes. It was observed for the  $M_w$  8.8 earthquake that the effects of liquefaction diminished further away from the riverside. Observed lateral displacement from the  $M_w$  8.8 earthquake agreed well with calculated values from most common predictive methods. This case history provides an assessment of bridge foundation soil performance with respect to existing methods and data that can be included in future liquefaction databases.

## ACKNOWLEDGMENTS

We thank LMMG Geotecnia for providing testing equipment and personnel for this project.

## REFERENCES

- ASTM International (2020). *ASTM D5778-12, Standard Test Method for Electronic Friction Cone and Piezocone Penetration Testing of Soils*, West Conshohocken, PA.
- Barlett, S.F., and Youd, T.L. (1995). "Empirical prediction of liquefaction-induced lateral spread." *J. Geotech. Engrg.*, 121, 316-329.



- Boroschek, R., and Contreras, V. (2012). "Strong ground motion from the 2010 Mw 8.8 Maule Chile earthquake and attenuation relations for Chilean subduction zone interface earthquakes." *Proc. of the International Symposium on Engineering Lessons Learned from the 2011 Great East Japan Earthquake* Tokyo, Japan.
- Boroschek, R., Soto, P., and Leon, R. (2010). "Registros de terremoto, 27 de febrero 2010." *Informe Renadic 10/03*, Universidad de Chile.
- Bray, J., and Frost, D. (2010). *Geo-engineering reconnaissance of the 2010 Maule, Chile earthquake*, GEER report N° GEER-022.
- Cetin, K. O., Seed, R.B., Kiureghian, A.D., Tokimatsu, K., Harder, L.F., Kayen, R.E., and Moss, R.E.S. (2004). "Standard penetration test-based probabilistic and deterministic assessment of seismic soil liquefaction potential." *J. Geotech. Geoenviron. Eng.*, 130(12), 1314–1340.
- Cetin, K.O., Seed, R.B., Kayen, R.E., Moss, R.E.S., Bilge, H.T., Ilgac, M., and Chowdhury, K. (2018). "The use of the SPT-based seismic soil liquefaction triggering evaluation methodology in engineering hazard assessments." *Methods X*, 5, 1556-1575.
- Cetin, K.O., and Seed, R.B. (2004). "Nonlinear shear mass participation factor ( $r_d$ ) for cyclic shear stress ratio evaluation." *Soil Dyn. And Earth. Eng.*, 24, 103-113.
- Elnashai, A.S., Gencturk, B., Kwon, O., Al-Qadi, I. L., Hashash, Y., Roesler, J. R., Kim, S. J., Jeong, S., Dukes, J., and Valdivia, A. (2011). *The Maule (Chile) earthquake of February 27, 2010. Consequence assessment and case studies*, Mid-America Earthquake Center, Report N°. 10-04.
- Gutierrez, A., and Ledezma, C. (2007). "Dynamic modeling of Mataquito Bridge affected by liquefaction-induced lateral spreading." *Obras y Proyectos*, 21, 13-18.
- Hamada, M., Towhata, I., Yasuda, S., and Isoyama, S. (1987). "Study on permanent ground displacement induced by seismic liquefaction." *Computers and Geotechnics*, 4, 197-220.
- Ishihara, K. (1985). "Stability of Natural Deposits During Earthquakes." *Proc. 11th Int. conf. on Soil Mechanics and Foundation Engineering*, 1.
- Iwasaki, T., Tasuoka, F., Tokida, K., and Yasuda, S. (1978). "A practical method for assessing soil liquefaction potential based on case studies at various sites in Japan." *Proc. of the 2nd Int. Conf. on microzonation*, San Francisco, Cal., 885-896.
- Kayen, R., Moss, R.E.S, Thompson, E.M., Seed, R.B., Cetin, K.O., Kiureghian, A.D., Tanaka, Y., and Tokimatsu, K. (2013). "Shear-Wave Velocity Based Probabilistic and Deterministic Assessment of Seismic Soil Liquefaction Potential." *J. of Geotechnical and Geoenvironmental Engineering*, 139(3).
- Ledezma, C., Hutchinson, T., Ashoford, S.A., Moss, R., Arduino, P., Bray, J.D., Olson, S., Hashash, Y.M.A, Verdugo, R., Frost, D., Kayen, R. and Rollins, K. (2012). "Effects of ground failure on bridges, roads, and railroads." *Earthquake Spectra*, 28(S1), 119-143.
- Liu, J., Li, R., Zhang, S., Bai, W., and Li, Z. (2021). "Study on seismic response in deeply deposited saturated liquefiable soil reinforced by using subarea long.short gravel piles." *Appl. Sci.* 2021, 11, 11271.
- Maurer, B.W., Green, R.A., and Taylor, O.D. (2015). "Moving towards and improved index for assessing liquefaction hazard: Lessons from historical data." *Soils and Foundations*, 55(4), 778-787.
- Mavroulis, S., Triantafyllou, I., Karavias, A., and Gogou, M. (2021). "Primary and secondary environmental effects triggered by the 30 October 2020, Mw = 7.0, Samos (eastern Aegean sea, Greece) earthquake based on post-events field surveys and InSAR analysis." *Appl. Sci.* 2021, 11, 3281.
- Moss, R.E.S, Seed, R.B, Kayen, R.E., Stewart, J.P., Der Kiureghian, A., and Cetin, K.O. (2006). "CPT-based probabilistic and deterministic assessment of in situ seismic soil liquefaction potential." *J. of Geotechnical and Geoenvironmental Engineering*, 132(8), 1032.
- Petrus Consultores. (2006). *Complementary soil mechanics report, Mataquito Bridge* (in Spanish) Chile.
- Robertson, P.K., and Wride, C.E. (1997). "Cyclic liquefaction and its evaluation based on the SPT and CPT." *Proc. of the 1996 NCEER Workshop on Evaluation of Liquefaction Resistance of Soils*, Edited by T.L. Youd and I.M. Idriss.
- R.W. Boulanger, and I.M. Idriss. (2014). *CPT and SPT based liquefaction triggering procedures*, Report No. UCD/CGM-14/01, Center for Geotechnical Modeling, Department of Civil and Environmental Engineering, University of California, Davis, USA.
- Van Ballegooy, S., Malan, P., Lacrosse, V., Jacka, M.E., Cubrinovski, M., Bray, J.D, O'Rourke, T.D., Crawford, S.A., and Cowan, H. (2014). "Assessment of liquefaction-induced land damage for residential Christchurch." *Earthquake Spectra*, 30(1), 31-55.
- Yen, W. P., Chen, G., Buckle, I., Allen, T., Alzamra, D., Ger, J., and Arias, J.G. (2011). *Post-Earthquake reconnaissance report on transportation infrastructure: Impact of the February 27, 2010, offshore Maule earthquake in Chile*, Report N°. FHWA-HRT-11-030.



- 
- Youd, T. L., and Garris, C. T. (1995). "Liquefaction-induced ground- surface disruption." *J. Geotech. Eng.*, 10.1061/(ASCE), 121(11), 805–809.
- Youd, T.L., and Perkins, D.M. (1987). "Mapping of liquefaction severity index." *J. Geotech. Engrg.*, 113, 1374-1392.
- Youd T.L., Hansen C.M., and Bartlett S.F. (2002). "Revised multilinear regression equations for prediction of lateral spread displacement." *J. of Geotech. and Geoenv. Eng. 11*, 128(12), 1007-1017.
- Zhang, G., Robertson, P.K, and Brachman, R.W.I. (2002). "Estimating liquefaction-induced ground settlements from CPT for level ground." *Can. Geotech. J.*, 39, 1168-1180.
- Zhao J. X., Zhang J., Asano A., Ohno Y., Oouchi T., Takahashi T., Ogawa H., Irikura K., Thio H. K., Somerville P. G., Fukushima Y., and Fukushima Y. (2006). "Attenuation relations of strong ground motion in Japan using site classification based on predominant period." *Bull. Seis. Soc. Am.*, 96, 898-913.



# INTERNATIONAL JOURNAL OF GEOENGINEERING CASE HISTORIES

*The Journal's Open Access Mission is  
generously supported by the following Organizations:*

**dar**

**Geosyntec**<sup>®</sup>  
consultants  
engineers | scientists | innovators

**CONETEC**



**ENGEO**  
— Expect Excellence —

Access the content of the *ISSMGE International Journal of Geoengineering Case Histories* at:  
<https://www.geocasehistoriesjournal.org>